Self-lubricating in a Pd-based bulk-metallic glass by the in-situ formation of an amorphous / nanocrystal structure layer during dry sliding

Nengbin Hua^{a,d,*}, Dehu Geng^{a,d}, Youxiong Ye^b, Zhenlong Liao^c, Qianting Wang^{a,d}, Pinqiang Dai^{a,d}, Hui Fang^{a,d}, Lei Zhang^{a,d}, and Peter K. Liaw^b

- ^a Department of Materials Science and Engineering, Fujian University of Technology, 350118

 Fuzhou, China
- ^b Department of Materials Science and Engineering, The University of Tennessee, 37996–2200

 Knoxville, TN, USA
- ^c Department of Materials Science and Engineering, Beihang University, 100191 Beijing, China
- ^d Fujian Provincial Key Laboratory of Advanced Materials Processing and Application, Fujian

 University of Technology, 350118 Fuzhou, China

Abstract

Lowering the high coefficient of friction (COF) of metals under dry sliding is technically challenging owing to the sliding-induced plastic deformation underneath the wear surface and surface roughening. The development of novel low-friction and even self-lubrication metals is crucial in engineering applications. In the present work, dry-sliding behaviors of the Pd- and Zr-based bulk-metallic glasses (BMGs) were investigated. Unexpectedly, the Pd-based BMG exhibits the 2-fold smaller COF and 100-fold lower wear rate than those of the Zr-based BMG, although the Pd-based BMG shows the smaller hardness and fracture toughness. The unprecedented stable low COF of 0.32 for the Pd-based BMG stems from the formation of an

amorphous/ultrafine nanocrystalline structure layer on the wear-scar surface. The

frictional heat generated during the friction process causes the in-situ

nanocrystallization in the subsurface of the worn scar, which increases the hardness

and yield strength of the nanostructured layer. The self-lubrication effect is attributed

to the effective suppression of the sliding-induced plastic deformation and surface

roughening, owing to the highly stable amorphous/nanostructure layer that can inhibit

the strain localization under contact loading during repeated dry sliding. The thermal-

activation wear protection strategy offers a pathway for designing ultra-wear resistant

BMGs.

Keywords: Bulk-metallic glass; Self-lubrication; In-situ nanocrystallization; Dry

friction; Microstructure of subsurface

Corresponding authors:

Nengbin Hua, who will handle the correspondence at all stages of paper reviews,

publication, and post-publication.

School of Materials Science and Engineering,

Fujian University of Technology,

Fuzhou 350118,

China

Email: flower1982cn@126.com

Tel: +86-0591-2286-3279; Fax: +86-0591-2286-3279

2

D	4.		
Dec	larations	of interest	٠

None.

1. Introduction

Generally, the frictional coefficients of metallic materials under dry-sliding conditions are relatively high (in the range of 0.6 to 1.2) [1]. During the dry-friction process, the inhomogeneous plastic deformation occurs below the contact surface of metallic materials, which leads to the roughening of the alloy surface and the falling-off of the friction layer, resulting in the relatively high frictional coefficient [2]. Reducing the grain size of metallic materials to a nanoscale or even amorphous phase significantly enhances their hardness, but the steady-state frictional coefficient of metallic materials remains almost unchanged [2-6]. As one of the main causes for the failure of metallic materials, frictional wear seriously affects the reliability and longevity of mechanical components and leads to huge economic losses. Therefore, the development of novel low-friction and even self-lubrication metallic materials has brought about the widespread attention for scientific researchers over the past decades.

During the sliding process, complex physical and chemical reactions occur on the alloy surface, resulting in the composition redistribution and plastic deformation of the wear surface and subsurface, which leads to the formation of a friction layer exhibiting different microstructures and properties from the base material [7-14]. It has been proved that the friction layer is controlled by both friction-working conditions (external factors) and material microstructures (internal factors) and plays an important role in the wear behaviors of metallic materials [3-17]. Under certain friction-working conditions and material microstructures, metallic materials can form

a protective layer on the contact surface, which reduces the frictional coefficient and wear rate, that is, the self-lubrication effect [15-17]. According to the reported studies, friction-layer structures that have a beneficial effect on the self-lubricating behavior mainly include: ultrafine nanocrystalline structures [3-5,9-11], gradient-nanocrystalline structures, amorphization of nanocrystalline phases, nano-oxide particles, amorphous and ultrafine nanocrystalline structures, as described below.

- (1) Ultrafine nanocrystalline structures (with a crystalline size of less than 10 nm). For instance, owing to the improved surface hardness, nanocrystalline pure Ni and Ni-20Fe alloys exhibit low friction coefficients of 0.2 0.35 under low-speed and applied normal-load conditions [7,8]. However, the formation of ultrafine nanocrystalline structures does not necessarily correspond to a low frictional coefficient. Whether the ultrafine nanocrystalline friction layer can reduce the frictional coefficient or not mainly depends on the structural stability of the friction layer under a specific friction load and speed. Due to the limited plastic-deformation ability of the nanocrystalline friction layer for nanocrystalline Ni [7], Ti [3], Al [4], and Cu [5] metals and their alloys [9-11], surface roughening and the formation of brittle friction layers take place under high-speed and high-load friction conditions, and thus, the friction coefficients are as high as 0.6 0.8.
- (2) Gradient-nanocrystalline structure. The surface-gradient nanostructure has been fabricated by the surface-mechanical-attrition treatment (SMAT) or surface-mechanical-grinding treatment (SMGT) [18]. The external-loading results in strong plastic deformation on the surfaces of alloys, and the grain sizes of alloys

increase from the nanoscale to coarse-grain scale with the increase in the depth from the surface. Therefore, the strengths of gradient-nanostructure materials decrease in a gradient from the surface to the inside. The gradient structure can effectively inhibit the strain localization of the material under contact load, so as to avoid or delay the formation of cracks on the material surface during deformation [18-21]. For instance, under the 50-N load condition, the dry-friction coefficient of the Cu-Ag alloy decreased from 0.64 for the coarse-crystalline samples to 0.29 for the gradient-nanostructure samples, and the wear rate of the alloy decreased by an order of magnitude [3]. However, controversial results were found for the 304L stainless steel [22] and 718 alloy [23] under dry-friction conditions. The formation of the gradient-nanocrystalline-structure layer could not improve the wear resistance.

(3) Amorphization of the nanocrystalline phase. The amorphization of the nanocrystalline structures in the friction layer is conducive to the formation of a self-lubricating layer. For instance, martensitic and pearlitic steels exhibit a lamellar structure with a large number of interfaces and dislocations. The friction stress leads to the severe plastic deformation in the friction layer, which results in the decreases in the pearlitic interval spacing and the formation of a ferrite-cementite nano-lamellar structure. Meanwhile, the ferrite-cementite interface is amorphized, forming a self-lubricating layer, which is composed of nano-oxide particles and amorphous structures. Therefore, the frictional coefficients of the martensitic and pearlitic steels are significantly reduced [15,16]. Previous studies have dynamically observed the formation of amorphous debris during sliding by in-situ transmission electron

microscopy (TEM). The results confirmed that amorphization can effectively reduce the friction and wear [24]. The molecular dynamics (MD) simulation and atomic force microscopy (AFM) results also verified that amorphization in the friction layer contributes to the formation of nanoscale friction [25]. However, the content of the amorphous phase in the friction layer is difficult to control by the friction. So far, the effect of amorphization on self-lubrication has not yet been systematically studied.

- (4) Nano-oxide particles. Under a dry-friction condition, the frictional heat results in the chemical reaction and formation of nano-oxides in the friction layer of metallic materials. Therefore, the nano-oxide particles form a protective layer on the contact surface, which reduces the frictional coefficient and wear rate of samples. However, the protection effect of the nano-oxide layer is correlated with the type and size of oxide particles [26-28]. For instance, introducing third-body particles, such as Fe₂O₃, SnO₂, CuO, and Bi₂O₃ etc., on the dry-friction-contact surface of steel can generate self-lubricating effect, whereas the addition of Al₂O₃, Mn₂O₃, ZnO, SiO₂, and TiO₂ do not show beneficial effects on self-lubrication. Moreover, the Fe₂O₃ particles with a scale of 30 nm are prone to form a self-lubricating protective layer than those with a scale of 300 nm [28].
- (5) Amorphous and ultrafine nanocrystalline structures. Nanocrystals in the amorphous matrix can promote the generation of multiple shear bands, and the branching and blocking of shear bands, which can effectively improve the plasticity and toughness of metallic glasses. The toughening effect can be found in the deformation process of various bulk-metallic glass (BMG) systems [29-32]. The

suitable combination of the amorphous and nanocrystalline phases gives rise to the higher strength and plasticity for amorphous/nanocrystalline composites. It has been reported that a transition layer from the amorphous to coarse crystalline phase was formed on the surface of Zr-based BMGs after the laser-surface treatment. The frictional coefficient of the amorphous and nanocrystalline transition layer is significantly lower than that of pure amorphous or coarse crystalline zones [33]. Nevertheless, the lubrication mechanism of the amorphous and nanocrystalline composite structure is not yet clear.

In this paper, the dry-wear behaviors of the Pd- and Zr-based BMGs were investigated. It was found that although the Pd-based BMG exhibited lower hardness and fracture toughness than those of the Zr-based BMG, the Pd-based BMG showed the self-lubrication effect and displayed a smaller frictional coefficient and a 100-fold lower wear rate than those of the Zr-based BMG. We characterized the microstructures of the worn surface, subsurface, and matrix. It was discovered that in-situ nanocrystallization occurred in the subsurface of the worn scar during dry sliding. The formation of the amorphous and nanocrystalline composite structure significantly reduced the dry-sliding frictional coefficient, and the wear resistance of the Pd-based BMG was remarkably enhanced. Furthermore, the surface nanocrystallization and self-lubrication mechanism of the Pd-based BMGs were discussed. The findings in the present work offers a novel strategy for designing self-lubricating and ultra-wear resistant alloys.

2. Experimental

Master alloys with nominal compositions (in atomic percent) of the Pd₄₀Cu₃₀Ni₁₀P₂₀ and Zr₅₅Al₁₀Ni₅Cu₃₀ were prepared. The Pd₄₀Cu₃₀Ni₁₀P₂₀ (abbreviated as the Pd-based BMG) was made by the high-frequency induction melting of pure metal components in a quartz under a high-purity argon atmosphere. The Zr₅₅Al₁₀Ni₅Cu₃₀ (abbreviated as the Zr-based BMG) was fabricated by arc-melting the mixtures of pure metals in a water-cooled copper crucible under a Ti-gettered high-purity argon atmosphere. The alloy ingots were re-melted at least four times to ensure chemical homogeneity.

Cylindrical rods (Φ 2 × 50 mm³) for notch-toughness tests and plates (2 × 10 × 50 mm³) for hardness and wear experiments were prepared by injection copper-mold casting. Rectangular BMG plates were machined to a size of 1.8 × 10 × 10 mm³. The surfaces of alloy samples were polished, using the 2,000-grit silicon-carbide grinding paper, and then polished with a 1.0 - 2.5 μ m diamond paste.

The notch toughness of the Pd- and Zr-based BMGs was examined by a three-point-bending (3-PB) test with a span of 20 mm. The notch with a depth of about 1 mm and root radius of about 200 µm was cut by a slow diamond saw. Microhardness experiments were performed, using a Vickers microhardness tester (THVP-10), employing a load of 300 gf with a dwell time of 10 s. At least five indents were conducted on the BMGs to ensure the statistical reliability of the data.

Ball-on-disk reciprocating-sliding experiments were conducted on the surfaces of BMGs with a 3-mm radius Si_3N_4 ball as the coupled pair material. The applied normal

load was 40 N, the reciprocating-sliding speed was 2 m/min., and the sliding time is 30 min. The wear rate (W) was determined, based on the changes in mass (Δm) before and after each test, which can be expressed as:

$$W = \Delta m/(S \cdot P \cdot \rho) = \Delta V/(S \cdot P) \tag{1}$$

where ΔV is the wear volume loss, S is the sliding distance, and P is the applied normal load. The weight change of the specimen before and after each test (Δm) was determined, using a balance with an accuracy of \pm 0.0001 g.

The unidirectional-scratching experiments were conducted by a MST² micro-scratch tester. The diamond indenter was a spherical Rockwell one with a tip of 100 µm in radius. Scratches were made with a constant normal load of 10 N, a scratch length of 0.3 mm, and a scratch speed of 0.3 mm/min. After scratching, a GT-X optical interferometer was used to determine the wear volume loss of samples.

The topography and chemical composition of the worn surfaces and wear debris of samples after both reciprocating-sliding and unidirectional-scratching experiments were examined by scanning electron microscopy (SEM) equipped with the energy-dispersive X-ray spectrometry (EDS). The surface roughness of the worn surfaces was determined by an AFM.

The cross-sectional foil of the worn-scar region in the reciprocating-sliding and unidirectional-scratching experiments was prepared by the focused ion beam (FIB) lift-out technique along the depth direction. The cross-sectional microstructural characterization underneath the friction worn surface was performed, using a JEOL 2010 TEM.

The Pd-based BMG samples were annealed at the temperatures from 590 K to 620 K for 10 min. in a vacuum heat-treatment furnace to obtain the glassy/crystalline composite structure. After that, the structures of the annealed Pd-based BMGs were examined by the X-ray diffraction (XRD) and TEM techniques. Furthermore, the microhardness test was performed on the annealed BMG samples.

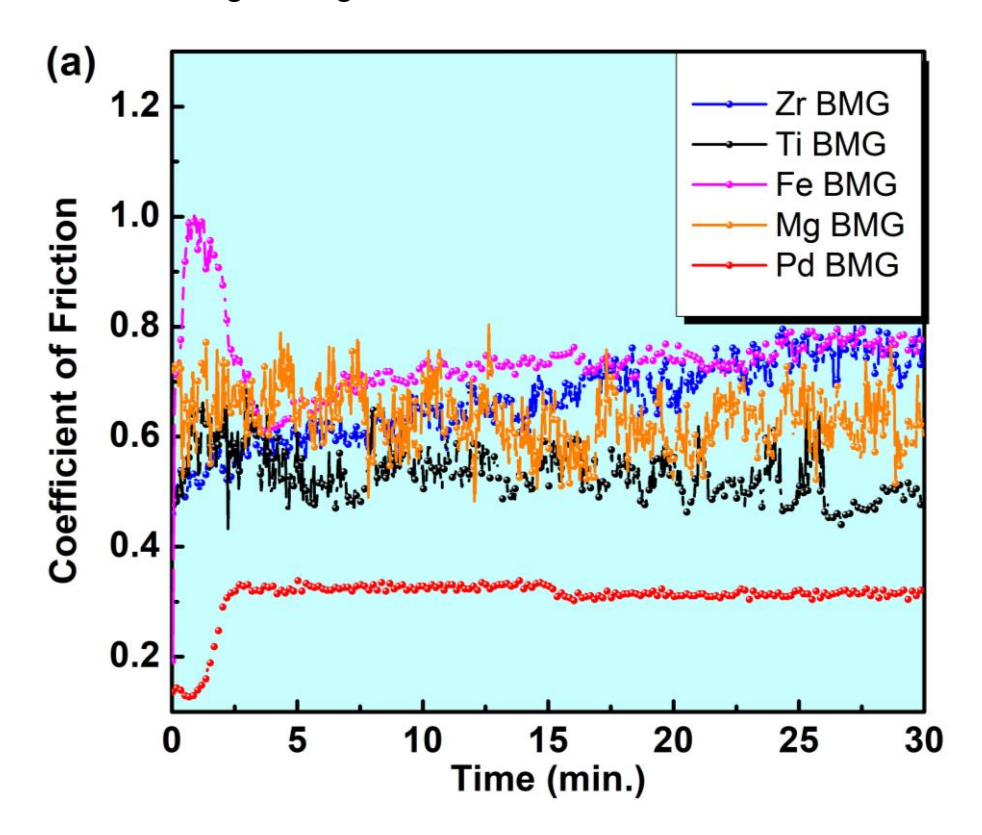
3. Results

3.1 Reciprocating sliding behaviors

Figure 1(a) shows the coefficients of friction (COFs) for various BMGs as a function of the sliding time under the reciprocating friction condition. It is seen that the steady-state COFs of the Mg-, Zr-, Ti-, and Fe-based BMGs are 0.67, 0.76, 0.54, and 0.75, respectively. Moreover, their fluctuation amplitude of COFs is about 0.1 during reciprocating sliding. The steady-state COF of the Pd-based BMG is about 0.32 with a fluctuation amplitude of about 0.02. Therefore, the COF and its fluctuation amplitude of the Pd-based BMG are much smaller than those of the other BMG systems, which indicates that the Pd-based BMG exhibits a good lubrication effect under a dry-sliding condition.

Figure 1(b) plots the wear rates of various BMGs as a function of their microhardness under the reciprocating friction condition. The wear rates of the Mg-, Zr-, Ti-, Fe-, and Pd-based BMGs are $4.20 \times 10^{-7} \text{ mm}^3 \cdot \text{mm}^{-1} \cdot \text{N}^{-1}$, $1.70 \times 10^{-7} \text{ mm}^3 \cdot \text{mm}^{-1} \cdot \text{N}^{-1}$, $7.60 \times 10^{-8} \text{ mm}^3 \cdot \text{mm}^{-1} \cdot \text{N}^{-1}$, $2.11 \times 10^{-8} \text{ mm}^3 \cdot \text{mm}^{-1} \cdot \text{N}^{-1}$, and $1.70 \times 10^{-9} \text{ mm}^3 \cdot \text{mm}^{-1} \cdot \text{N}^{-1}$, respectively. The microhardness of the Mg-, Zr-, Ti-, Fe-, and Pd-based BMGs are 245 Hv, 510 Hv, 750 Hv, 1,225 Hv, and 500 Hv, respectively.

Generally, the wear rate of the BMGs decreases with the increase in hardness. It is worth noting that although the microhardness of the Pd-based BMG is merely equivalent to that of the Zr-based BMG, the wear rate of the Pd-based BMG is about two orders of magnitude lower than that of the Zr-based BMG, and even lower than that of the Fe-based BMG with ultra-high hardness [as seen in the inset of Fig. 1(b)]. The above results further demonstrate that the Pd-based BMG has good friction-lubrication performance under the reciprocating dry-friction condition. In order to facilitate the comparison, we choose the Zr-based BMG as the reference sample in the following investigations.



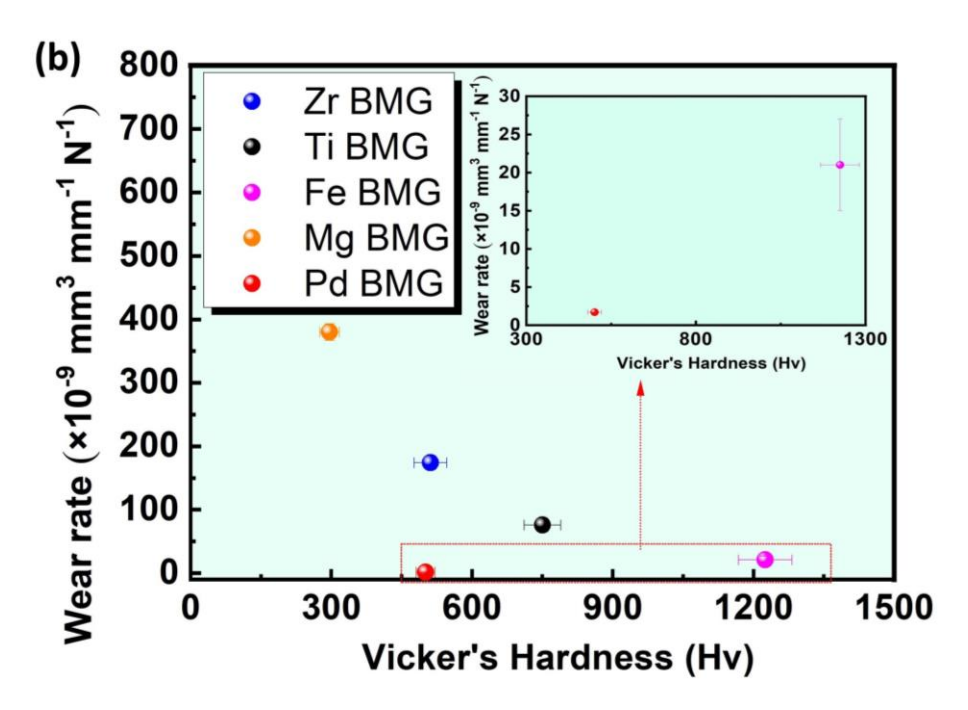
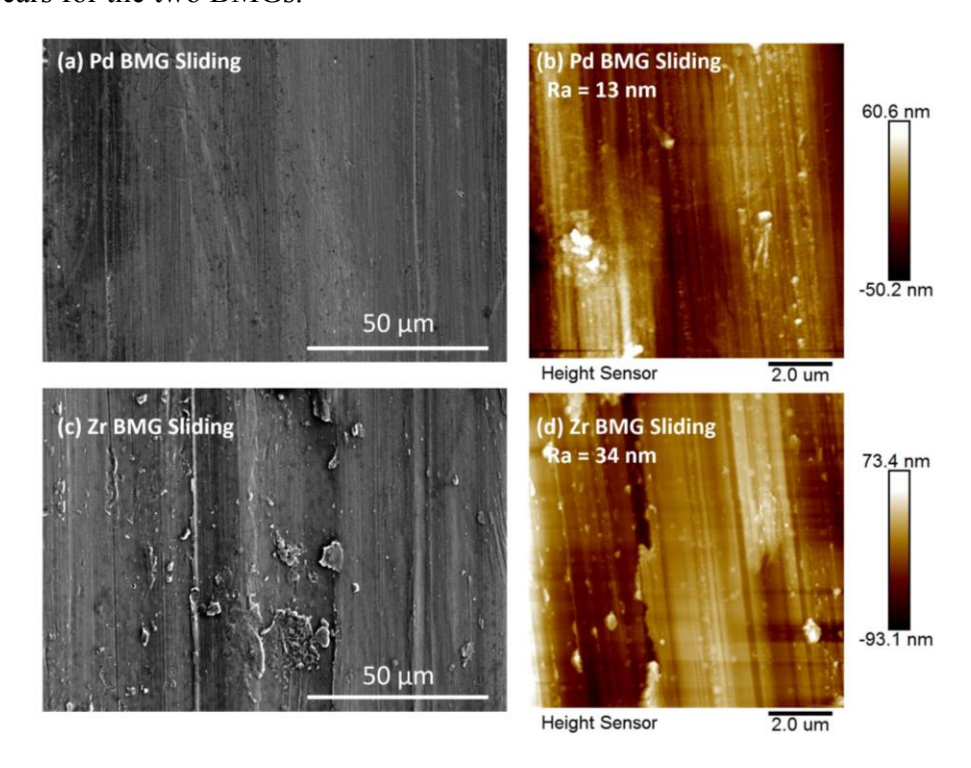


Fig. 1(a) Coefficients of friction for various BMGs as a function of sliding time under the reciprocating-friction condition. Fig. 1(b) Wear rates of various BMGs as a function of their microhardness under the reciprocating-friction condition. Inset illustrates the detailed wear performances of Pd- and Fe-based BMGs.

Figures 2(a) and (c) exhibit the SEM images of the wear-scar morphologies for the Pd- and Zr-based BMGs after the reciprocating-sliding experiment. Both worn scars of the Pd- and Zr-based BMGs display plough grooves parallel to the friction direction, indicating the abrasive wear mechanism under reciprocating sliding. As can be seen from Fig. 2(a), the worn scar of the Pd-based BMG has narrow and shallow grooves with a width of less than 1 µm. On the contrary, there are wider and deeper plough grooves (more than 10 µm) on the worn surface of the Zr-based BMG, as seen in Fig. 2(c). Moreover, some debris are rolled off and adhered to the surface of the wear trace for the Zr-based BMG. Figures 2(b) and (d) show the AFM images of the morphologies for the Pd-Zr-based **BMGs** after the wear-scar

reciprocating-sliding experiment. The surface roughness on the surface of the Pd-based BMG is 13 nm, while that of the Zr-based BMG is 34 nm. Thus, it is concluded that the higher wear rate corresponds to the larger surface roughness of wear scars for the two BMGs.



Figs. 2 [(a), (c)] SEM and [(b), (d)] AFM images of the wear-scar morphologies for the Pdand Zr-based BMGs after the reciprocating-sliding experiment.

Figure 3 illustrates the SEM images of the wear-debris morphology for the [(a), (b)] Pd- and [(c), (d)] Zr-based BMGs after the reciprocating friction. Figures 3(a) and 3(c) show that the irregular flake-like debris is formed for the two BMGs after sliding. The size of the wear debris of the Pd-based BMG is less than 20 μm, while that of the Zr-based BMG is about hundreds of μm. As seen in Figs. 3(b) and 3(d), ultrafine particles are dispersed on the wear debris surface of the Pd-based BMG, while distinct plastic deformation can be observed on the wear-debris surface of the Zr-based BMG.

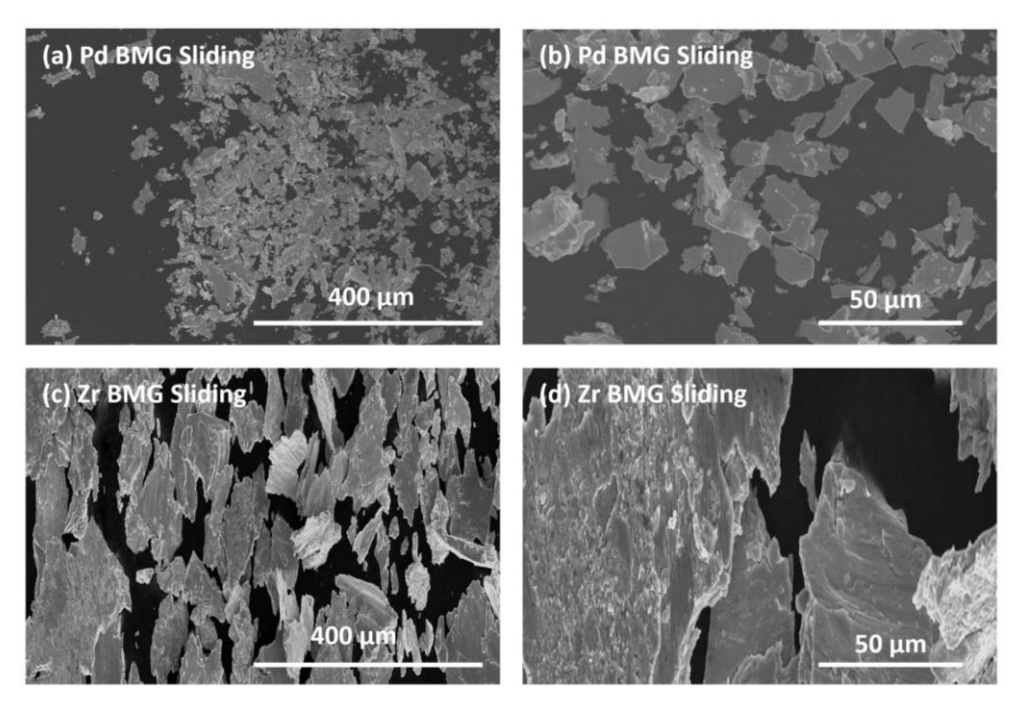


Fig. 3 SEM images of the wear-debris morphology for the [(a), (b)] Pd- and [(c), (d)]

Zr-based BMGs after the reciprocating friction.

Figure 4 presents the cross-sectional SEM images of the wear scar for the Pd-and Zr-based BMGs after the reciprocating friction. Figures 4(a) and 4(b) show that the wear scar of the Pd-based BMG is relatively flat without obvious surface peeling layers. There is a shear-plastic deformation layer with a thickness of about 50 μm below the worn scar surface. As seen from Figs. 4(c) and 4(d), the wear scar of the Zr-based BMG is rather rough, and there is an obvious surface-peeling layer on the wear-scar surface and a severe plastic deformation layer with a thickness of about 200 μm below the worn scar surface. The density of shear bands in the plastic deformation layer of the Zr-based BMG is significantly higher than that of the Pd-based BMG.

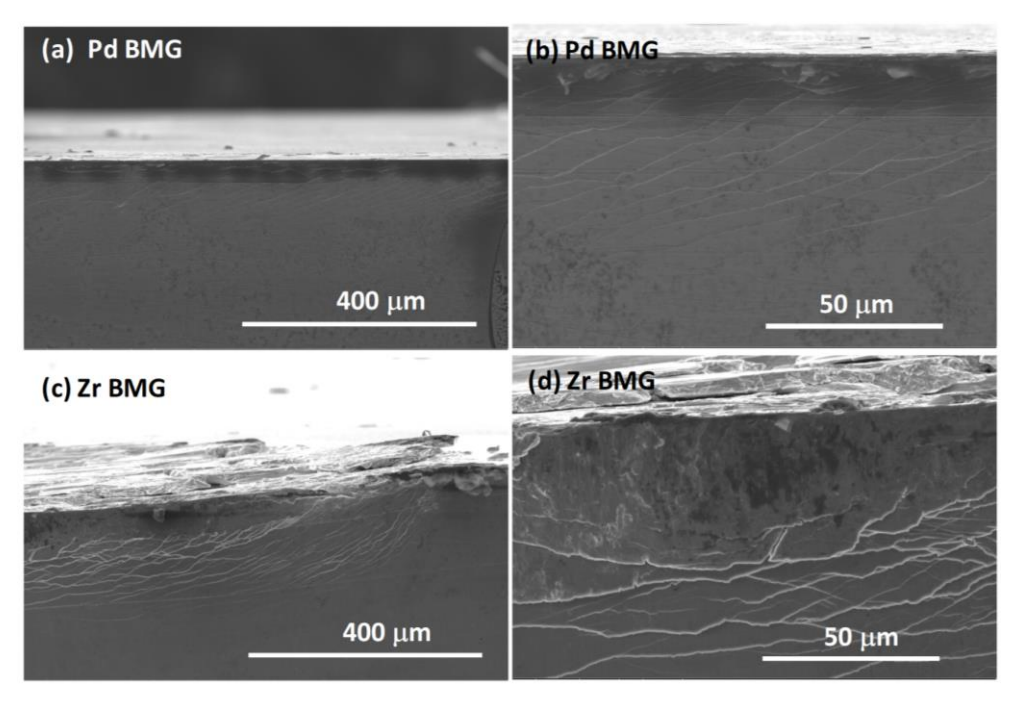


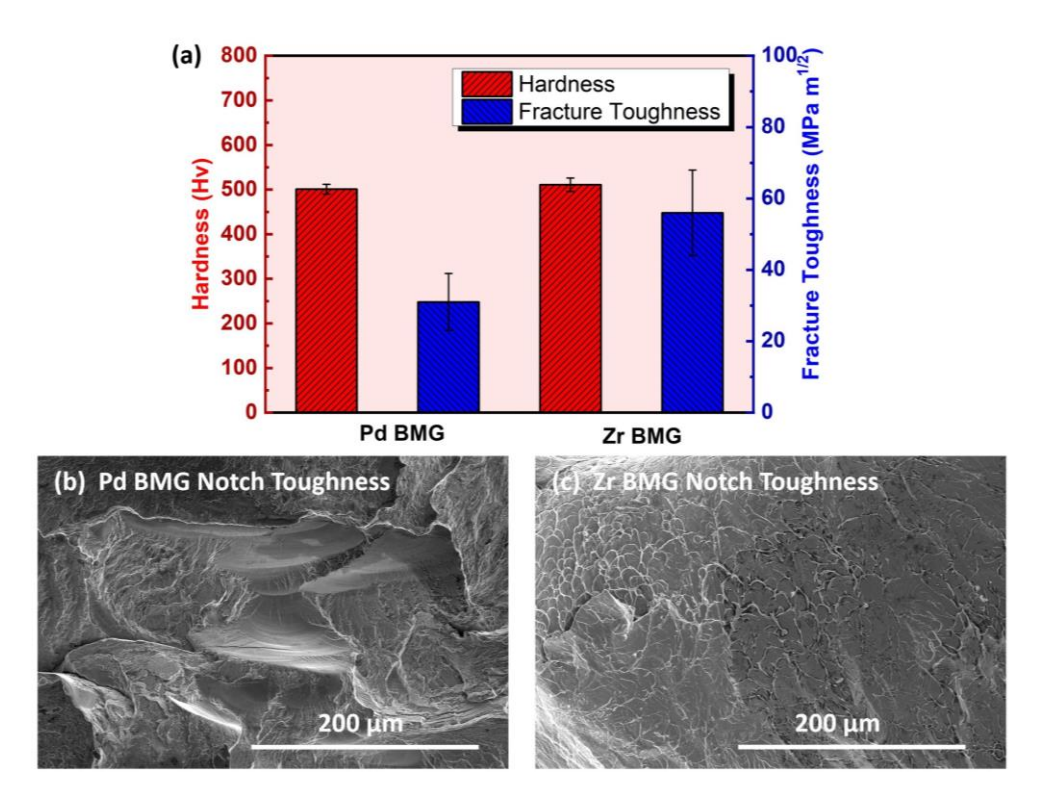
Fig. 4 The cross-sectional SEM images of the wear scar for the [(a), (b)] Pd- and [(c), (d)]

Zr-based BMGs after the reciprocating friction.

In recent years, great efforts have been devoted to exploring the relationship between the physical properties and wear resistance of materials [34-37]. It has been reported that the wear behavior is controlled by both the hardness and fracture toughness of materials. According to the classical-wear theory, high hardness of a material may reduce the plastic deformation on the surface, and thus, prevent the formation of microcracks [34,35]. Also, large fracture toughness can improve the resistance to the propagation of microcracks, and hence, mitigate the generation of wear debris [36,37].

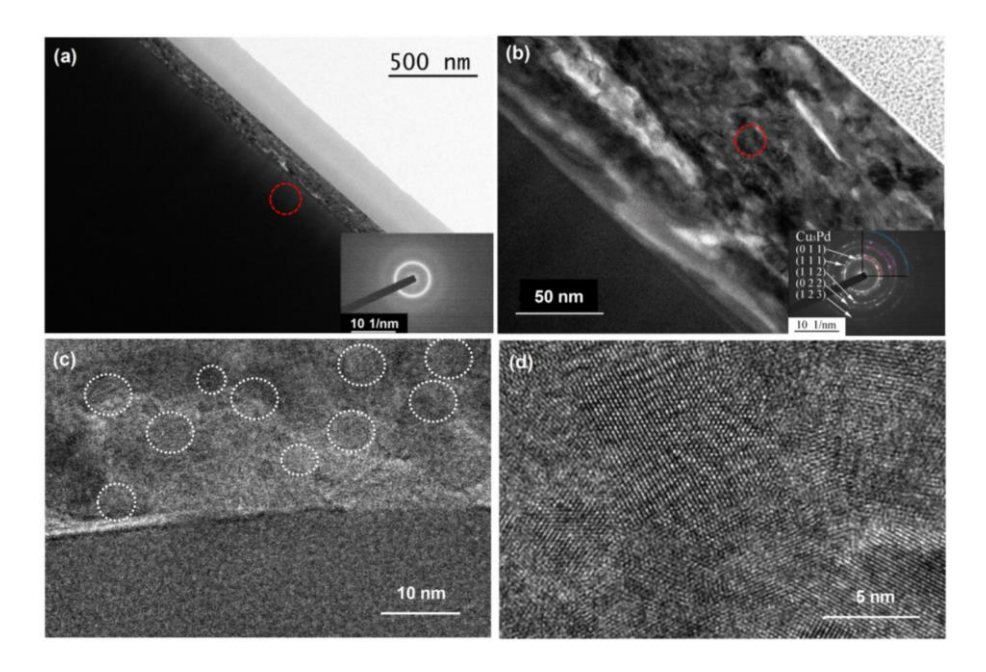
Figure 5(a) shows the hardness and fracture toughness of the Pd- and Zr-based BMGs. The hardness of the Pd-based BMG (500 Hv) is almost approaching that of the Zr-based BMG (510 Hv). However, the Pd-based BMG exhibits a fracture toughness of 30.98 MPa m^{1/2}, which is much less than that of 55.86 MPa m^{1/2} of the

Zr-based BMG. Figures 5(b) and 5(c) display the SEM images of fracture surfaces for notch-toughness tests on the Pd- and Zr-based BMGs, respectively. Some smooth fracture patterns can be observed on the Pd-based in Fig. 5(b), indicating a low toughness. In contrast, the dense vein patterns distributed on the fracture surface of the Zr-based BMG suggests its high toughness, as seen in Fig. 5(c). It is well-known that hardness and fracture toughness are two important factors affecting the wear resistance of materials. According to the previously reported empirical formula of wear resistance [34,38,39], the wear rate of the Pd-based BMG was expected to be larger than that of the Zr-based BMG, owing to the lower hardness and fracture toughness of the Pd-based BMG. Surprisingly, in the present study, the reciprocating-sliding wear rate of the Pd-based BMG is two orders of magnitude lower than that of the Zr-based BMG, which indicates the extremely high wear resistance of the Pd-based BMG.



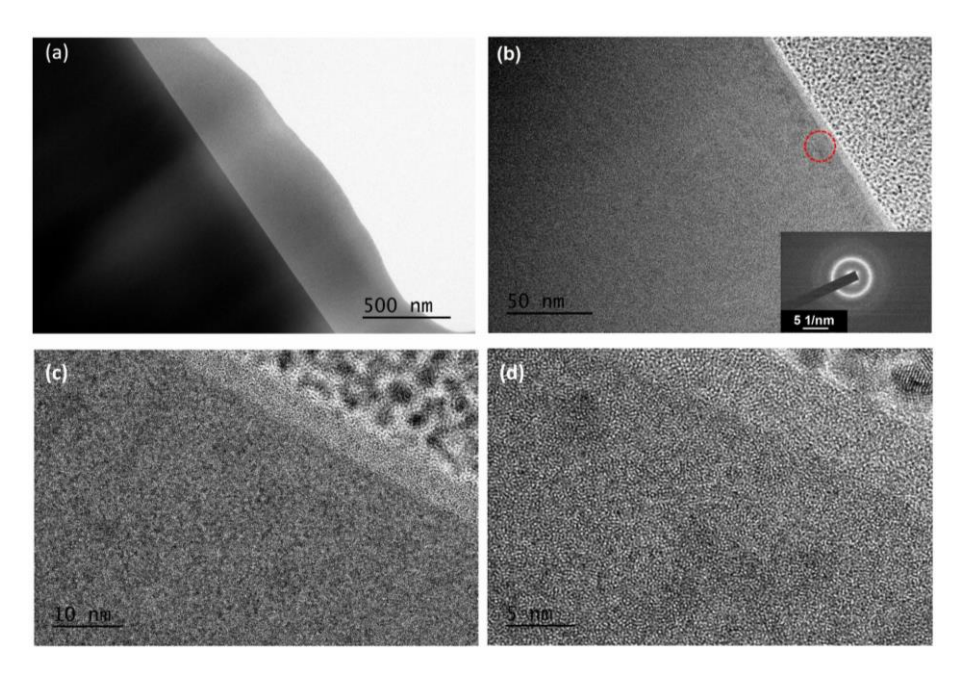
Figs. 5(a) The hardness and fracture toughness of the Pd- and Zr-based BMGs. The SEM images of fracture surfaces for the notch-toughness test on the (b) Pd- and (c) Zr-based BMGs.

Besides the hardness and fracture toughness, the microstructures of materials also played an important influence on the wear resistance [7-17]. To further study why the Pd-based BMG exhibits the self-lubrication effect and super-high wear resistance under a reciprocating-friction condition, the microstructures of the subsurface layers in wear scars for the two alloys were analyzed. Figure 6 displays the cross-sectional TEM images on the subsurface of the wear scar for the Pd-based BMG after the reciprocating-sliding test. Figure 6(a) demonstrates that there is a friction layer with a thickness of about 100 nm on the subsurface of the wear scar for the Pd-based BMG. The selected area electron diffraction (SAED) pattern in the inset indicates the amorphous structure of the matrix region below the friction layer. Figure 6(b) shows that the friction layer on the worn surface of the Pd-based BMG exhibits a nanocrystalline structure with severe plastic deformation. The SAED pattern in the inset of Fig. 6(b) further verifies the formation of the nanocrystalline Cu₃Pd phase in the friction layer. Figures 6(c) and 6(d) illustrate the high-resolution TEM images of the friction layer for the Pd-based BMG. The Cu₃Pd nanocrystals below 10 nm in size are distributed in the amorphous matrix of the friction layer. There are several studies reported that the Cu₃Pd phase formed during the crystallization of the Pd₄₀Cu₃₀Ni₁₀P₂₀ metallic glass [40-42].



Figs. 6(a) The cross-sectional TEM images in the subsurface of the wear scar for the Pd-based BMG after the reciprocating-sliding test. (b) The enlarged view of the friction layer on the subsurface of the wear scar. (c) The TEM image showing the nanocrystalline structure on the amorphous matrix. (d) The high-resolution TEM image of the Cu₃Pd nanocrystalline phase.

Figure 7 presents the cross-sectional TEM image of the subsurface of the wear scar for the Zr-based BMG after the reciprocating-sliding test. It is indicated from Figs. 7(a) and 7(b) that there is no nanocrystallization occurring on the subsurface of the wear scar for the Zr-based BMG during sliding. The SAED pattern in the inset of Fig. 7(a) confirms that the subsurface of the worn scar is amorphous. The high-resolution TEM images in Figs. 7(c) and 7(d) also demonstrate that no nanocrystalline phase can be observed on the subsurface of the Zr-based BMG.



Figs. 7(a) The cross-sectional TEM image of the subsurface of the wear scar for the Zr-based BMG after the reciprocating-sliding test. (b) The enlarged view of the subsurface of the wear scar. (c-d) The high-resolution TEM image showing the fully amorphous structure on the subsurface of the wear scar.

3.2 Unidirectional scratching behaviors

Figure 8(a) exhibits the schematic diagram of the unidirectional scratching experiment conducted on the glassy-alloy surface. A constant normal load of 10 N is applied on the diamond indenter, which is pressed into the glassy-alloy surface. Then, the scratch experiment is conducted on the surface of the glassy alloy at a certain linear velocity and leaves a scratch on the alloy surface. Figure 8(b) shows the wear rates of the Pd- and Zr-based BMGs under the unidirectional-scratching condition. The inset illustrates the variation of frictional coefficients with the scratching distances of the Pd- and Zr-based BMGs. The wear rate of the Pd-based BMG under the unidirectional-scratching condition is 8.93 × 10⁻⁵ mm³·mm⁻¹·N⁻¹, which is much larger than that of 2.23 × 10⁻⁵ mm³·mm⁻¹·N⁻¹ for the Zr-based BMG.

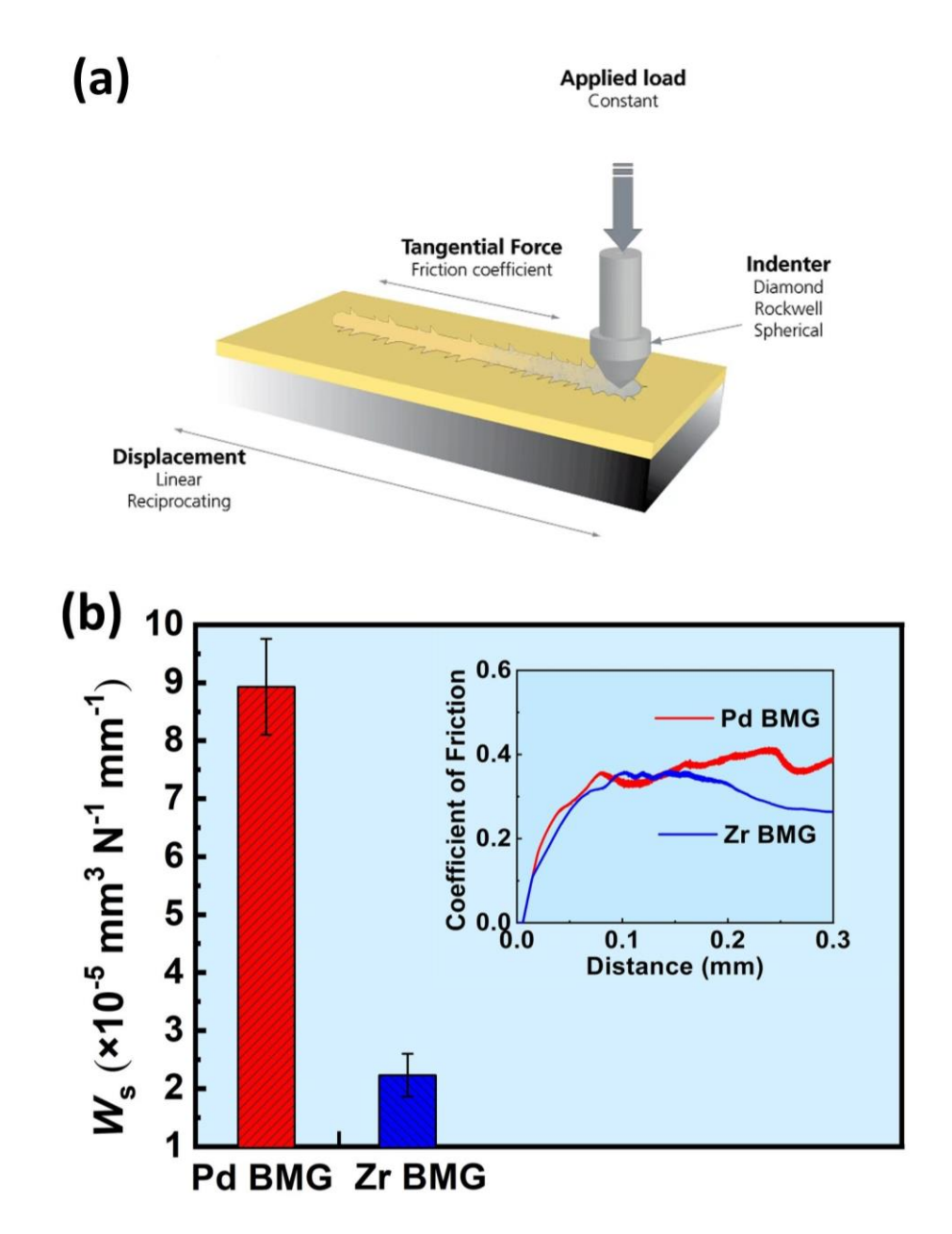


Fig. 8 (a) The schematic diagram of the unidirectional scratching experiment conducted on the glassy-alloy surface. (b) The wear rate of the Pd- and Zr-based BMGs under the unidirectional-scratching condition. The inset of Fig. 8(b) is the variation of frictional coefficients with the scratching distances of the two BMGs.

The frictional coefficients of the Pd- and Zr-based BMGs increase rapidly from 0 to about 0.37, as presented in the insets of Fig. 8(b). As the scratching experiment goes, the frictional coefficients of the Pd-based BMG fluctuate around 0.35. The

frictional coefficients of the Zr-based BMG vary around 0.28 and then decrease slightly. The fluctuation amplitude of the Zr-based BMG under the unidirectional-scratching condition is much smaller than that of the Pd-based BMG. The above results show that the wear resistance of the Pd-based BMG is inferior to that of the Zr-based BMG under unidirectional scraping, which is significantly different from the reciprocating-sliding behavior of the two alloys.

Figure 9 shows the SEM images of the wear-scar morphologies for the Pd- and Zr-based BMGs after the unidirectional-scratching measurement. Figures 9(a-c) and 9(d-e) are the SEM images of the wear scar for the Pd- and Zr-based BMGs, respectively. It can be seen from Fig. 9(a) that severe plastic deformation occurs at the edge of the wear scar for the Pd-based BMG after the indentation by the diamond-coupled part. With the unidirectional scratch of the diamond indenter, the shear force under the contact surface increases, which leads to the much serious plastic deformation on the alloy surface. Consequently, the microcracks occur and propagate, which gradually tear the thin deformation layer on the alloy surface into fragments, as illustrated in Fig. 9(b). Figure 10(c) displays that the wear debris undergoes an intense plastic deformation by the rolling of the couple-paired diamond indenter. It is noted that some of the wear debris are adhered to the tail of the worn scar in a "fish scale" like shape.

Figures 9(d) and 9(e) also show that severe plastic deformation occurs in the wear scar of the Zr-based BMG, and some debris adheres to the tail of the wear scar after unidirectional scratching. However, Fig. 9(f) demonstrates that various shear

bands produced by intense plastic deformation are distributed along the wear scar edges of the Zr-based BMG. No obvious cracks and torn debris can be found on the surface of the worn scar. This trend is mainly because the Zr-Al-Ni-Cu BMG exhibits superior fracture toughness to that of the Pd-Cu-Ni-P BMG, as presented in Fig. 5, which guarantees the Zr-based BMG greater capacity to resist crack propagation [34-38].

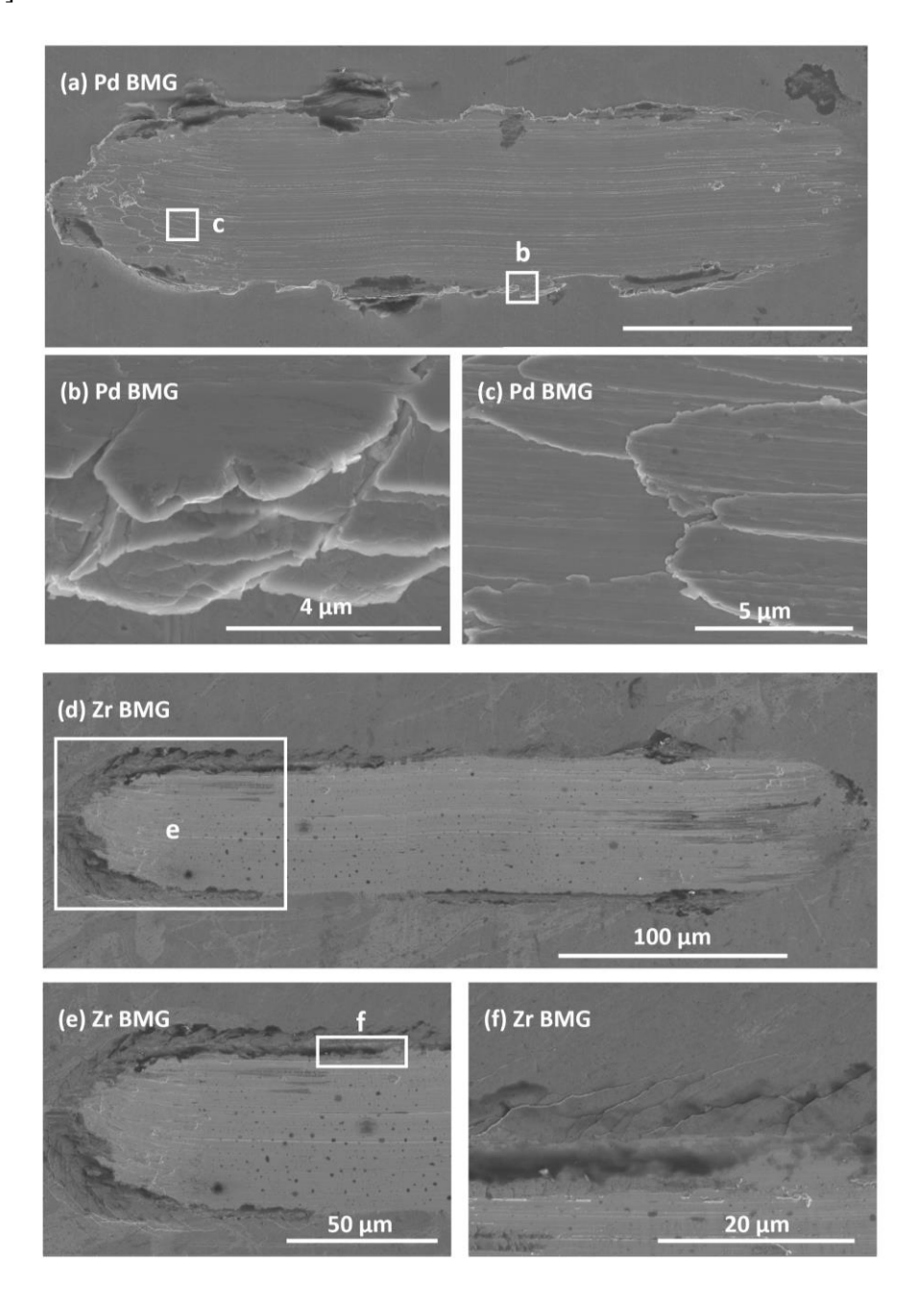


Fig. 9 SEM images of the wear-scar morphologies for the Pd- and Zr-based BMGs after the unidirectional-scratching measurement. (a) The overall wear-scar morphology for the Pd-based BMG. (b-c) The enlarged views of the wear scar in the square regions of b and c in Fig. 9(a). (d) The overall wear-scar morphology for the Zr-based BMG. (e) The enlarged view of the wear scar in the square region of e in Fig. 9(d). (f) The enlarged view of the wear scar in the rectangle region of ???? Fig. 9(e).

Figure 10(a) exhibits the cross-sectional TEM image on the subsurface of the wear scar for the Pd-based BMG after unidirectional scratching. No nanocrystallization can be observed on the subsurface of the worn scar. The SAED pattern in the inset shows that the subsurface of the worn scar remains an amorphous structure after scratching. The high-resolution TEM image in Fig. 10(b) further confirms the glassy structure of the subsurface. Similarly, the amorphous structure is maintained on the subsurface of the worn scar for the Zr-based BMG after unidirectional scratching, as illustrated in the TEM images in Figs. 10(c) and 10(d).

Therefore, it can be inferred that the self-lubrication performance and exceptionally high wear resistance of the Pd-based BMG in the reciprocating-sliding experiment is closely related to the amorphous/nanocrystalline composite structure in the subsurface of the wear scar. However, there are critical issues. Why does the nanocrystallization of the Pd-based BMG only appear in the reciprocating-sliding experiment? Why is there no nanocrystallization in the Zr-based BMG under the same reciprocal friction condition? and How does the in-situ nanocrystallization provide self-lubrication effect for the Pd-based BMG during reciprocating-sliding?

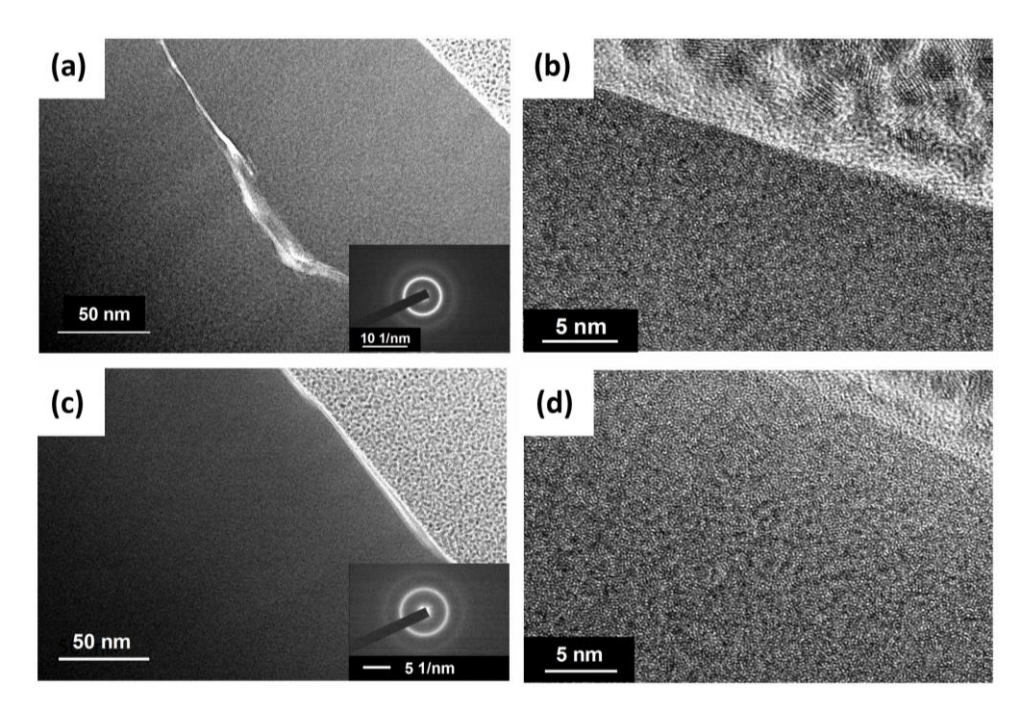


Fig. 10 The cross-sectional TEM images on the subsurface of the wear scar for the [(a), (b)]

Pd- and [(c), (d)] Zr-based BMGs after unidirectional scratching.

4. Discussion

4.1 Effect of deformation on the nanocrystallization in the Pd-based BMG

Because both the temperature and deformation can lead to the nanocrystallization of amorphous alloys, the crystallization mechanism can be mainly classified into two categories: one is the thermo-induced crystallization [29,32], and the other is the deformation-induced crystallization [30,31,43-46]. Therefore, we investigate the effects of both the deformation and temperature on the crystallization of the amorphous alloy, to reveal the nanocrystallization mechanism of the Pd-based BMG during reciprocating sliding in the present work.

It has been reported that the highly localized deformation on the alloy surface during sliding contact may lead to the surface-microstructural evolution. In-situ

nanocrystalization occurred in various BMG systems by bending deformation, nanoindentation, compression/tension, and cold rolling, and so on [30-32,43-45]. The precipitation of nanocrystals resulted in the enhancement of plasticity for the metallic glasses (MGs) [30-32,43-45]. Nanocrystals in the amorphous matrix can promote the generation, branching, and intersection of multiple shear bands, which can effectively improve the plasticity and toughness of metallic glasses. The toughening phenomenon has been found during the deformation of various BMGs, such as Al-based, Zr-based, Cu-based, Fe-based, Ni-based, and Pd-based alloys [30-32,43-46]. In addition, it has been reported that the microstructural combination of the glassy matrix and nanocrystalline phase is beneficial to the wear resistance. For instance, the surface or coating of Zr-based, Ni-based, and Fe-based alloys with an amorphous and nanocrystalline composite structure exhibits excellent wear resistance [47-50]. The improvement of the plasticity for BMGs strongly depends on the structure, composition, size, volume fraction, and spatial distribution of nanocrystals.

In order to better understand the stress and deformation on the material surface and subsurface during the sliding contact, the stress-field distribution caused by the spherical contact under the sliding friction was evaluated. Hamilton [48] deduced a set of stress-field equations of the material subsurface under a sliding spherical contact condition, based on the elastic contact theory. With the attempt of simplifying the model, they assumed that the material surface has an ideal geometric structure, neglecting the influence of rough contact and roughness on the stress field. However, these equations Please define these equations!! have been demonstrated to allow good

estimation for stress fields under sliding spherical contacts where plastic deformation occurs [11,55].

The material parameters used in the simulation are listed as follows: The Young's moduli of the Pd-based BMG, Zr-based BMG, Si₃N₄, and diamond are 100 GPa [34], 87 GPa [34], 324 GPa [52], and 1,141 GPa [53], respectively. The Poisson's ratios of the Pd-based BMG, Zr-based BMG, Si₃N₄, and diamond are 0.404 [34], 0.369 [34], 0.26 [52], and 0.07 [53], respectively. The densities of the Pd-based BMG, Zr-based BMG, Si₃N₄, and diamond are 9.26 g/cm³ [34], 6.69 g/cm³ [34], 3.23 g/cm³ [52], and 3.5 g/cm³ [54], respectively. In the reciprocating friction experiment, the radius of the Si₃N₄ sphere is 3 mm, the frictional coefficient of the Pd-based BMG is 0.32, and that of the Zr-based BMG is 0.66. In the unidirectional scratching test, the radius of the diamond sphere is 100 μm, the frictional coefficients of the Pd- and Zr-based BMGs are 0.35 and 0.28, respectively. Owing to the significance of shear or deformation energy in the deformation-induced crystallization [55], the distribution of the Von-Mises stress in the contact area of friction pairs was simulated by the Hamilton analysis model [48].

According to the Hertz-contact model [51,55], when only the normal force is applied without sliding, the maximum shear stress distribution below the contact point is axisymmetric, and the maximum stress is located at the depth of about 1/2 of the contact radius of the indented specimen below the contact surface. In the process of sliding or scratching, the stress field becomes asymmetric due to the introduction of a tangential force. Figure 11 shows the Von-Mises stress field distribution in the

subsurface of the contact area between the BMGs and coupled pairs. During the reciprocating-sliding process, due to the introduction of the friction force on the surface of the Pd-based BMG, both the compressive stress at the front of the contact zone and the tensile stress at the rear edge of the contact zone increase. Meanwhile, the maximum stress under the contact surface increases, and its original position moves toward the sliding direction and elevates toward the closer contact surface. The value of the maximum stress is 1.19 GPa for the Pd-based BMG under the reciprocating-sliding condition, as shown in Fig. 11(a). The distribution of the Von-Mises stress of the Zr-based BMG in the reciprocating-friction experiment is similar to that of the Pd-based BMG. When the tangential force is introduced in the positive X direction, the stress inside the material increases, and the maximum stress area rises toward the surface. A new high-stress area appears at the rear edge of the sliding contact, as described in Fig. 11(b). A relatively high frictional coefficient ($\mu =$ 0.66) of the Zr-based BMG results in the occurrence of the maximum-stress region on the sliding surface and the contact rear edge. The maximum stress is approaching 1.95 GPa. The maximum stress takes place at the rear edge of the contact surface and then sharply decreases, which indicates that the plastic deformation occurs in a thin layer close to the surface. By comparing Figs. 11(a) and 11(b), one can come to a conclusion that the maximum stress and the stress gradient under the contact zone of the Zr-based BMG are much greater than those of the Pd-based BMG. This trend leads to a larger plastic deformation on the subsurface of the Zr-based BMG. Accordingly, the surface of the Zr-based BMG is much susceptible to the microcrack

generation and wear debris peeling-off, which consequently results in the larger wear damage.

Figures 11(c) and 11(d) present the Von-Mises stress distribution beneath the friction contact area of the Pd- and Zr-based BMGs in the unidirectional scratching tests. There are two high stress zones in the Pd-based BMG, which are located below and at the rear edge of the contact area, respectively. The value of the maximum stress is about 4.9 GPa. Due to the relatively low friction ($\mu = 0.28$), the maximum stress of the Zr-based BMG lies below the contact surface, and the maximum stress value is about 4.2 GPa. It is seen that the maximum stress and the stress gradient of the Zr-based BMG are lower than those of the Pd-based BMG, which leads to the smaller plastic deformation and wear volume of the Zr-based BMG in the unidirectional scratching tests. The distribution of the Von-Mises stress field of the two alloys corresponds well with their results reciprocating-sliding in unidirectional-scratching experiments. According to the microstructural analysis of a subsurface layers of the Pd- and Zr-based BMGs after friction experiments, the nanocrystallization of the subsurface layer of the alloy samples only occurs for the Pd-based BMG under the reciprocating-sliding condition, in which the lowest maximum stress was generated. Thus, it is reasonable to infer that the effect of stress and deformation is not the principal cause for the nanocrystallization of the subsurface layer during the friction and wear process of the Pd-based BMG.

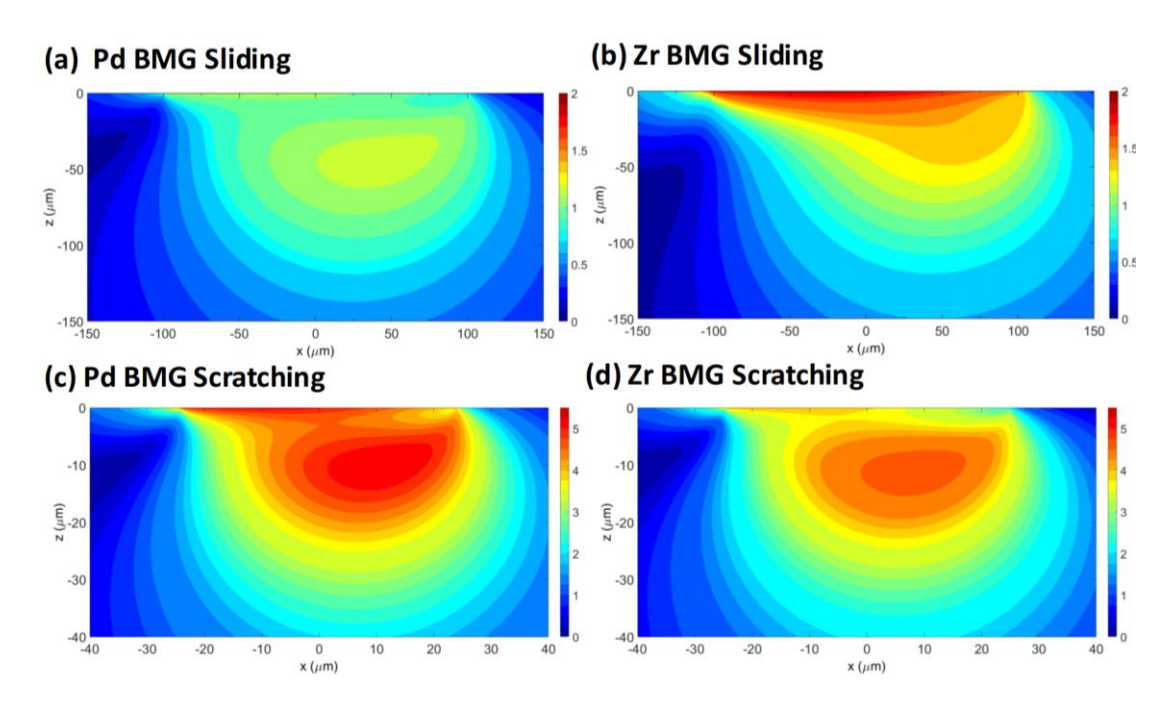


Fig. 11 The Von-Mises stress distribution beneath the friction-contact area. (a) Pd- and (b)

Zr-based BMGs in the reciprocating-sliding tests. (c) Pd- and (d) Zr-based BMGs in the

unidirectional-scratching tests.

4.2 Effect of frictional heat on the nanocrystallization in the Pd-based BMG

BMGs are usually fabricated by the non-equilibrium solidification, and therefore, they are thermodynamically metastable. Under certain conditions, the amorphous structure of BMGs can change to a crystalline state, which is the crystallization occurs. It is not a sentence. Please rewrite it. Through investigating the isothermal-crystallization behavior of the Zr-based and CuZr-based BMGs, it was found that the key to thermal-induced crystallization lies in a precise control of heat-treatment conditions (such as the crystallization temperature, holding time, cooling rate, etc.) to optimize the microstructures and mechanical properties of amorphous and nanocrystalline composites [29,30].

It has been reported that the friction-induced temperature rise on the contact surface can alter the surface microstructure, and hence, influence their wear performance [15-17]. As a result, we study whether the friction can generate enough heat to change the microstructure of the alloy surface under the present experimental conditions. Based on the one-dimensional transient heat-flow analysis, Kannel and Barber [56] had proposed a model for frictional heating, in which the friction heat generated in the contact area, as well as the heat conduction and convection to the material surface were studied. Particularly, their model fits well with the pin-on-disk friction and time-averaged single-cycle heat-transfer conditions. According to the model, the maximum temperature induced by frictional heating takes place on the surface of the sample. The local temperature rise, ΔT , on the material surface can be expressed as follows:

$$\Delta T = \frac{Q_A}{h_s} \left\{ 1 - erfc \left[h_s \sqrt{\frac{t}{K\rho c}} \right] \exp \left[\frac{h_s^2 t}{K\rho c} \right] \right\}$$
 (2)

in which h_s is the convection heat transfer coefficient in air ($\sim 20 \text{ W} \cdot \text{m}^{-2} \cdot \text{K}^{-1}$) [11], t is the time, K is the thermal conductivity, ρ is the density, c is the specific heat, and Q_A is the frictional heat power per unit area, which can be described as:

$$Q_A = \frac{\mu P v}{A_s} \tag{3}$$

in which μ is the coefficient of friction, P is the normal load, v is the friction-sliding rate, and A_s is the surface area of the wear scar. In the present study, the thermal conductivity, specific heat, and density of the Pd-based BMG are 5 W·m⁻¹·K⁻¹, 313 J·Kg⁻¹·K⁻¹, and 9,260 Kg·m⁻³, respectively [57,58]. Meanwhile, the thermal

conductivity, specific heat, and density of the Zr-based BMG are $5.83~\rm W\cdot M^{-1}\cdot K^{-1}$, $361~\rm J\cdot Kg^{-1}\cdot K^{-1}$, and $6,650~\rm Kg\cdot m^{-3}$, respectively [59].

The Kannel and Barber's model simplified the process of friction and wear. The radial transmission of the friction heat from the contact point to the sample was neglected. Only the normal heat transfer to the sample was considered. Furthermore, the model neglected the evolution of the surface temperature to a steady-state condition during the friction experiment and estimated the upper limit temperature of the specimen surface. According to Equation (2), the temperature of the sample surface increases steadily with time. Therefore, we estimate the temperature of the alloy surface at the end of the experiment as the upper limit temperature that the sample surface can reach. In the present study, the sliding rate is 0.033 m s⁻¹, and the friction time is 1,800 s. The coefficient of friction is measured by the tribometer. Deducing by Equation (2), the upper limit temperature rise of the Pd-based BMG in the reciprocating-sliding and unidirectional-scratching experiments are 394 K and 2.2 K, respectively. The upper limit temperature rise of the Zr-based BMG in the reciprocating-sliding and unidirectional-scratching tests are 230 K and 2.3 K, respectively.

The ambient temperature during the friction experiments is about 298 K. According to the theoretical model of the friction-contact temperature, the surface temperatures of wear scars for the Pd- and Zr-based BMGs in the reciprocating-sliding and unidirectional-scratching experiments are listed in Table 1. Under reciprocating sliding, because the Pd-based BMG exhibits a relatively lower

glass-transition temperature ($T_g = 569 \text{ K}$) and crystallization temperature ($T_x = 653 \text{ K}$), the contact temperature of the friction pair during sliding can reach above the glass-transition temperature or even exceed its crystallization temperature. However, the Zr-based BMG shows a higher glass transition temperature ($T_g = 683 \text{ K}$) and crystallization temperature ($T_x = 773 \text{ K}$). Moreover, the Zr-based BMG has a lower upper-limit temperature of the alloy surface, which is much lower than its glass-transition temperature.

Table 1 The surface temperatures of wear scars (T_s) , glass-transition temperatures (T_g) , crystallization temperatures (T_x) , COF, and wear rates for the Pd-based and Zr-based BMGs in the reciprocating-sliding and unidirectional-scratching experiments.

Alloys	$T_{ m g}$	$T_{\rm x}$	Friction	COF	Wear rate	$T_{\rm s}$
	(K)	(K)	conditions		(×10 ⁻⁹ /mm ³ ·mm ⁻¹ ·N ⁻¹)	(K)
$Pd_{40}Cu_{30}Ni_{10}P_{20}$	569	653	Reciprocating	0.32	1.7	692
			sliding			
			Unidirectional	0.35	8930	300
			scratching			
Zr ₅₅ Al ₁₀ Ni ₅ Cu ₃₀	683	773 -	Reciprocating	0.66	170	528
			sliding			
			Unidirectional	0.28	2230	300
			scratching			

Under the unidirectional-scratching conditions, the upper limit temperature rise of the Pd- and Zr-based BMGs are 2.2 K and 2.3 K, respectively, which are determined according to the theoretical model of the friction-contact temperature. During the friction process, the surface temperatures of the wear scars of both BMGs

are much lower than their glass-transition temperature. Thus, the friction temperature rise on the alloy surface is not enough to cause the nanocrystallization under the unidirectional-scratching condition. The TEM analysis results in Fig. 10 show that nanocrystallization did not occur on the subsurface of wear scars for the two BMGs after unidirectional-scratching tests. It has been reported that the plastic deformation of amorphous alloys may lead to nanocrystallization [30,31,43-46]. However, the stress on the contact interface of the Pd-based BMG in the unidirectional scratching test is much greater than that under the reciprocating-sliding condition. Furthermore, there is no nanocrystallization on the subsurface of wear scars, which indicates that the stress and deformation are not the main reasons for the nanocrystallization. Previous studies have shown that by isothermally annealing metallic glasses at the temperatures above their T_g , nanocrystals or microcrystals can be precipitated from the amorphous matrix [29,32]. In addition, there are several studies reporting that nanocrystals or microcrystals formed during the annealing of the Pd-based metallic glasses [40-42]. Therefore, it can be demonstrated that the nanocrystallization of the Pd-based BMG is related to the surface-temperature rise caused by the frictional heat under the reciprocating-sliding process.

4.3 Mechanism of self-lubrication for nanocrystallization in the Pd-based BMG

To examine the effect of the glassy/crystalline composite structure on the microhardness, the Pd-based BMG samples were annealed at various temperatures from 590 K to 620 K for 10 min. in a vacuum heat-treatment furnace. Figure 12(a) exhibits the microhardness of the Pd-based BMG as a function of the annealing

temperatures. It can be seen that the microhardness of the Pd-based BMG increases slightly with the increase in the temperature range from 580 K to 610 K, which is mainly due to the annihilation of the free volume for the Pd-based BMG under the thermal action. When the heat-treatment temperature rises to 620 K, the microhardness of the Pd-based BMG increases greatly from about 540 Hv for 610 K to 680 Hv for 620 K. Figure 12(b) shows the XRD patterns of the Pd-based BMG annealed at various temperatures from 590 K to 620 K. When the heat-treatment temperature is below 610 K, the XRD patterns of the Pd-based BMG still retain a unique hump peak of an amorphous state. However, when the heat-treatment temperature reaches 620 K, there are obvious crystallization peaks in the XRD pattern of the Pd-based BMG. The crystallization peaks are determined as Cu₃Pd, Ni₂Pd₂P, Ni₃P, Cu₅Pd₃P₂, and other crystalline phases. Figure 13(c) illustrates the TEM image of the Pd-based BMG after heating at 620 K, and the inset is the SAED pattern in Fig. 12(c). It is seen that complex crystalline phases are precipitated in the amorphous matrix of the Pd-based glassy alloy, and the grain size ranges from tens to hundreds of nm. The SAED pattern also shows the complex polycrystalline structure. Therefore, the significant increase of microhardness of the Pd-based BMG after annealing at 620 K is mainly due to the precipitation of complex crystalline intermetallic phases in the amorphous matrix. Furthermore, it is worthy of mentioning that annealing the Pd-based BMG at 620 K for 10 min. can result in the formation of multi-intermetallic phases. Thus, it is reasonable that the exposure time of 30 min. during the

reciprocating sliding experiment is enough to trigger crystallization for the Pd-based BMG.

Figure 13 presents the schematic diagram of the evolution of the temperature, stress, and microstructure for the (a) Pd-based BMG and (b) Zr-based BMG in the subsurface of wear scars during the reciprocating friction. It can be seen from Fig. 13(a) that the temperature of the wear-scar surface for the Pd-based BMG decreases along the depth direction. As listed in Table 1, the surface temperature of the Pd-based BMG reaches 692 K, which is higher than its glass-transition temperature of 569 K and crystallization temperature of 653 K. Therefore, during the friction and wear process, due to thermal activation, nanocrystallization occurred on the subsurface of the Pd-based BMG, and nano-sized Cu₃Pd crystals were precipitated from the glassy matrix, resulting in a significant increase in the surface hardness.

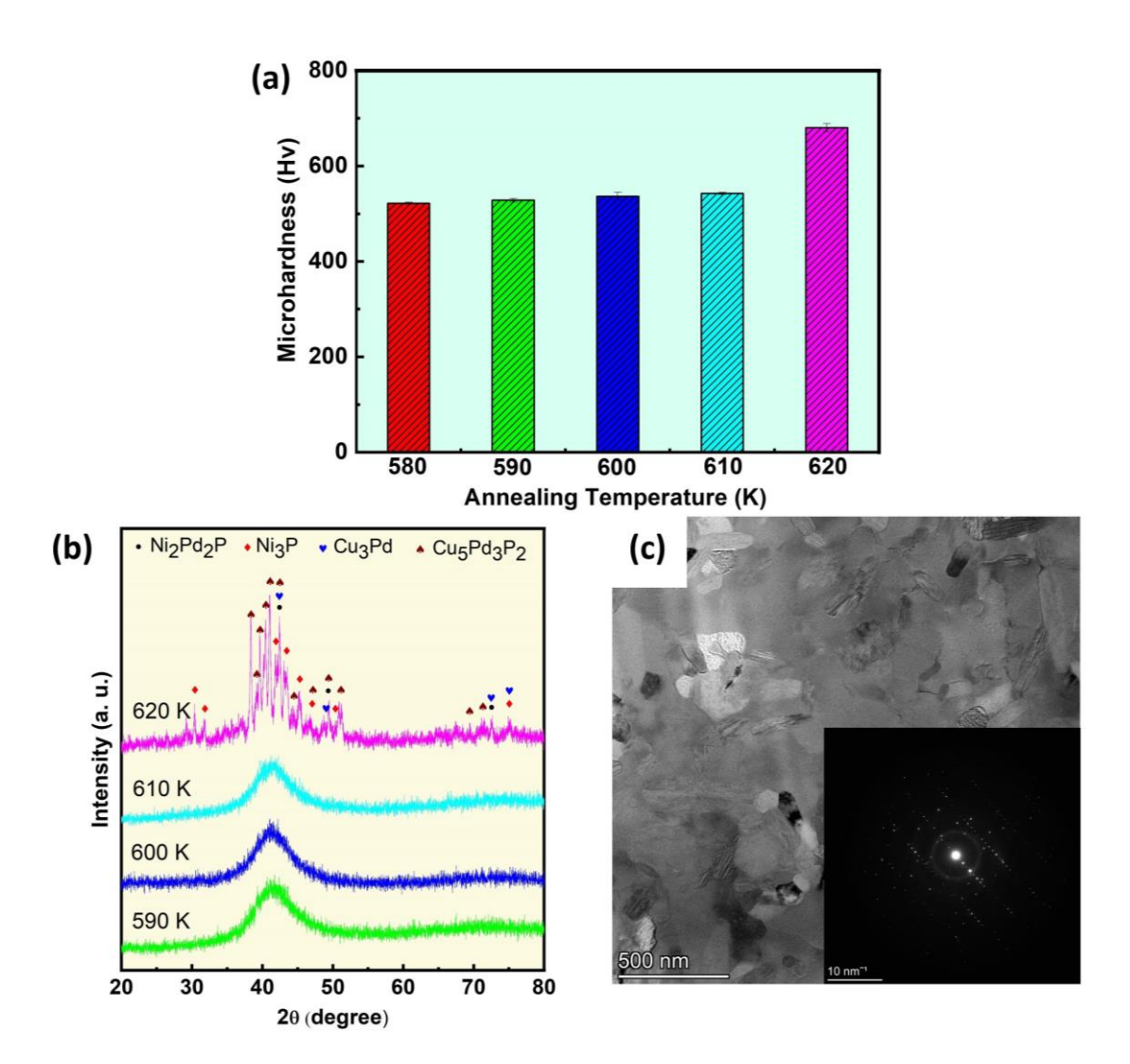


Fig. 12(a) Microhardness of the Pd-based BMG as a function of the annealing temperature.

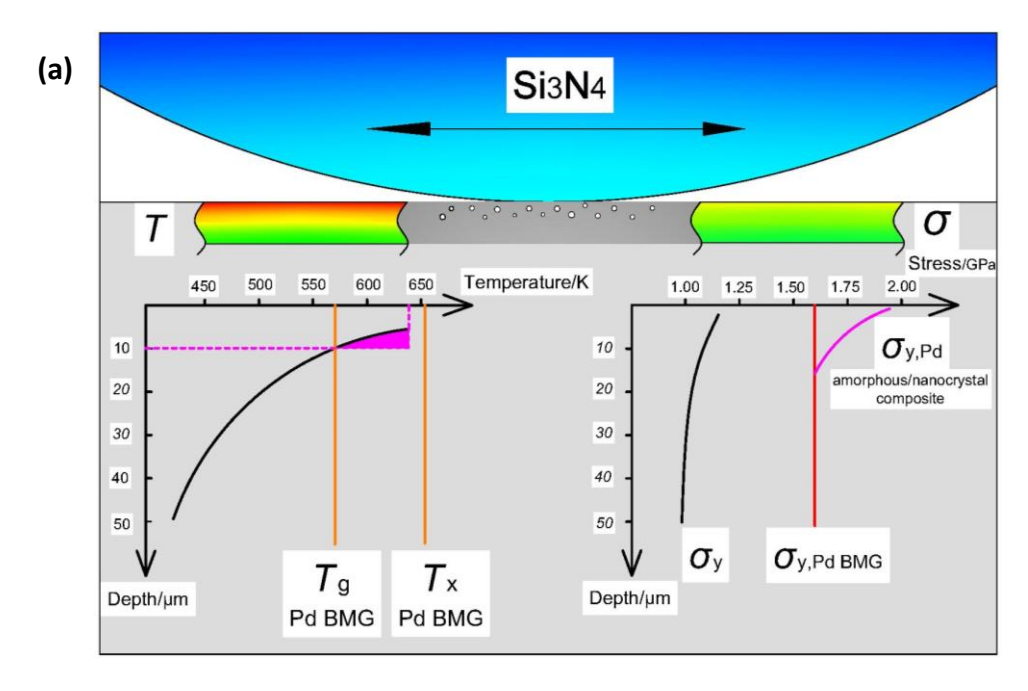
(b) XRD patterns of the Pd-based BMG annealed at various temperatures from 590 K to 620 K. (c) TEM image and SAED pattern (inset) of the Pd-based BMG after heating at 620 K.

The hardness of the Pd-based BMG after the heat treatment at 620 K reaches 680 Hv. According to the strength-hardness equation [60], it is calculated that the yield strength of the 620 K heat-treated Pd-based BMG can approach 1.9 GPa. The right inset shows the applied stress as a function of the depth from the wear-scar surface. It is calculated from Fig. 11 that the maximum stress on the surface of the Pd-based BMG is about 1.1 GPa. With the increase in the depth, the applied stress gradually

decreases, and the stress reduces to about 1 GPa at a depth of 50 µm from the surface, as indicated in Fig. 11(a). The yield strength of the Pd-based BMG is about 1.6 GPa, and the yield strength of the amorphous/nanocrystalline composite surface layer is calculated as approaching 1.9 GPa, both of which are much higher than the applied stress on the surface of the Pd-based BMG during the friction process. Therefore, under the reciprocating sliding, the amorphous/nanocrystalline composite layer of the Pd-based BMG plays an important effect on reducing the friction and wear.

Figure 13(b) shows that the temperature of the Zr-based BMG also decreases along the depth direction from the wear scar surface. Table 1 illustrates that the friction-surface temperature of the Zr-based BMG is 528 K, which is lower than its glass-transition temperature of 683 K and crystallization temperature of 773 K. Therefore, in the process of friction and wear, the friction heat cannot cause surface crystallization, and the surface of the Zr-based BMG still retains an amorphous structure. From the relation of the applied stress as a function of the depth from the wear surface in the right inset, it can be seen from Fig. 11(b) that the maximum stress on the surface of the Zr-based BMG is about 2.0 GPa. With the increase in the depth, the applied stress gradually decreases, and at a depth of 50 μm from the surface, the applied stress is approximately 1 GPa. The yield strength of the Zr-based BMG is about 1.7 GPa [61], which is lower than the applied stress on the material surface during the friction process. Therefore, under the condition of reciprocating friction, the Zr-based BMG undergoes plastic deformation, forms shear bands, and the shear

bands expand to form microcracks and cracks, resulting in the flake-like wear debris falling off, and thus, severe wear occurs.



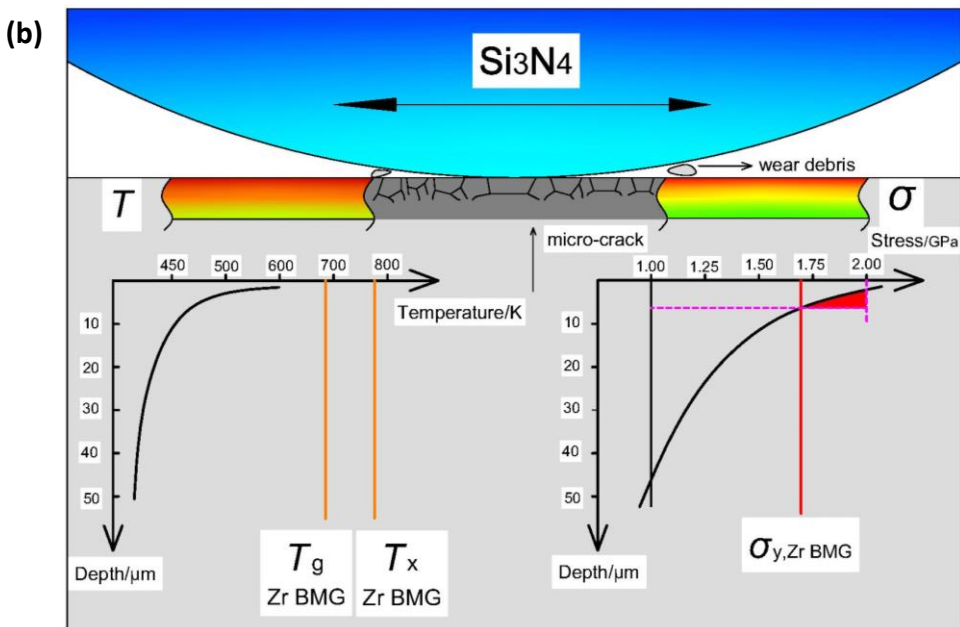


Fig. 13 The schematic diagrams of the evolution of temperature, stress, and microstructure for the (a) Pd-based BMG and (b) Zr-based BMG in the subsurface of a wear scars\ during reciprocating friction.

5. Conclusions

In the present work, the dry reciprocating-sliding and unidirectional-scratching behaviors of the Pd- and Zr-based bulk-metallic glasses (BMGs) were investigated. The following are the primary conclusions:

- (1) Under the dry reciprocating sliding, the Pd-based BMG exhibits the remarkably lower COF and wear rate than those of the Zr-based BMG, although the Zr-based BMG shows an almost equivalent hardness and a higher toughness in comparison with those of the Pd-based BMG. However, under the unidirectional scratching, the Pd-based BMG displays the higher COF and wear rate than those of the Zr-based BMG.
- (2) The unprecedented stable low COF and high wear resistance of the Pd-based BMG stems from the in-situ formation of a layer with an amorphous/ultrafine nanocrystalline composite structure underneath the wear scar surface during the dry-reciprocating sliding. However, no in-situ nanocrystallization occurs underneath the wear scar surface of the Pd-based BMG during the unidirectional scratching, and the Pd-based BMG shows an inferior wear resistance to that of the Zr-based BMG.
- (3) The distribution of the Von-Mises stress in the contact area of friction pairs simulated by a Hamilton analysis model reveals that the effect of stress and deformation is not the primary cause for the nanocrystallization of the subsurface layer during the dry-sliding process of the Pd-based BMG. The maximum temperature induced by frictional heating deduced by the Kannel and Barber's model demonstrates that the surface temperature of the Pd-based BMG is higher than its

crystallization temperature, which results in the nanocrystallization of the subsurface layer during the dry sliding.

(4) The amorphous/nanocrystalline composite surface layer exhibits a higher yield strength than the applied stress on the surface of the Pd-based BMG during the dry sliding, which can effectively suppress the sliding-induced surface roughening and formation of a delaminating tribolayer and contributes to the exceptionally high wear resistance. The thermal activation wear protection strategy offers a pathway for designing self-lubricating and ultra-wear resistant BMGs

Data availability

The raw/processed data required to reproduce these findings cannot be shared at this time as the data also forms part of an ongoing study.

Acknowledgement

The present work was supported by the Scientific Research Project of the Fujian Provincial Department of Science and Technology (2021H0023 and 2022L3062), and the Scientific Research Project of the Fujian University of Technology (GY-Z21032 and GY-Z20057). PKL very much appreciates the support from the National Science Foundation (DMR_-_22226508, 1611180, and 1809640) with program directors, Drs. J. Madison, J. Yang, G. Shiflet, and D. Farkas.

References

- [1] X. Chen, Z. Han, X. Li, K. Lu, Lowering coefficient of friction in Cu alloys with stable gradient nanostructures, Sci. Adv. 2 (2016) 1601942.
- [2] D.A. Rigney, S. Karthikeyan, The evolution of tribomaterial during sliding: A brief introduction, Tribol. Lett. 39 (2010) 3-7.
- [3] M. Wen, C. Wen, P.D. Hodgson, Y.C. Li, Tribological behaviour of pure Ti with a nanocrystalline surface layer under different loads, Tribol. Lett. 45 (2012) 59-66.
- [4] Z.N. Farhat, Y. Ding, D.O. Northwood, A.T. Alpas, Effect of grain size on friction and wear of nanocrystalline aluminum, Mater. Sci. Eng. A. 206 (1996) 302-313.
- [5] Y.S. Zhang, Z. Han, K. Wang, K. Lu, Friction and wear behaviors of nanocrystalline surface layer of pure copper, Wear 260 (2006) 942-948.
- [6] N.B. Hua, W.Z. Chen, W.G. Wang, H.T. Lu, X.Y. Ye, G.H. Li, C. Lin, X.F. Huang. Tribological behavior of a Ni-free Zr-based bulk metallic glass with potential for biomedical applications, Mater. Sci. Eng. C 66 (2016) 268-277.
- [7] S.V. Prasad, C.C. Battaile, P.G. Kotula, Friction transitions in nanocrystalline nickel, Scripta Mater. 64 (2011) 729-732.
- [8] H.A. Padilla II, B.L. Boyce, C.C. Battaile, S.V. Prasad, Frictional performance and near-surface evolution of nanocrystalline Ni-Fe as governed by contact stress and sliding velocity, Wear 297 (2013) 860-871.
- [9] X. Chen, Z. Han, K. Lu, Enhancing wear resistance of Cu-Al alloy by controlling subsurface dynamic recrystallization, Scripta Mater. 101 (2015) 76-79.
- [10] F. Ren, S.N. Arshad, P. Bellon, R.S. Averback, M. Pouryazdan, H. Hahn, Sliding

- wear-induced chemical nanolayering in Cu-Ag, and its implications for high wear resistance, Acta Mater. 72 (2014) 148-158.
- [11] T.J. Rupert, C.A. Schuh, Sliding wear of nanocrystalline Ni-W: Structural evolution and the apparent breakdown of Archard scaling, Acta Mater. 58 (2010) 4137-4148.
- [12] G.Y. Lin, Y.F. Peng, Y.S. Li, H.Z. Liang, Z.L. Dong, Y.H. Zhou, Z.M. Yue, J. Zhang, D.B. Xiong, D. Zhang, Remarkable anisotropic wear resistance with 100-fold discrepancy in a copper matrix laminated composite with only 0.2 vol% graphene, Acta Mater. 215 (2021) 117092.
- [13] X.L. An, Z.D. Liu, L.T. Zhang, Y. Zou, X.J. Xu, C.L. Chu, W. Wei, W.W. Sun, A new strong pearlitic multi-principal element alloy to withstand wear at elevated temperatures, Acta Mater. 227 (2022) 117700.
- [14]C. Liu, Z.M. Li, W.J. Lu, Y. Bao, W.Z. Xia, X.X. Wu, H. Zhao, B. Gault, C.L. Liu, M. Herbig, A. Fischer, G. Dehm, G. Wu, D. Raabe, Reactive wear protection through strong and deformable oxide nanocomposite surfaces, Nat. Commun. 12 (2021) 5518.
- [15] C.H. Yin, Y.L. Liang, Y. Liang, W. Li, M. Yang, Formation of a self-lubricating layer by oxidation and solid-state amorphization of nano-lamellar microstructures during dry sliding wear tests, Acta Mater. 166 (2019) 208-220.
- [16] C.H. Yin, X.M. Qin, S.B. Li, Y.L. Liang, Y. Jiang, H. Sun, Amorphization induced by deformation at ferrite-cementite nanointerfaces in a tribolayer and its effect on self-lubricating, Mater. Des. 192 (2020) 108764.

- [17] C.H. Yin, S.B. Li, Y.L. Liang, A review on microstructure evolution in a friction-induced layer and the self-lubricating behavior during dry sliding friction of steels, Mater. Rep. 34 (10) (2020) 19134-19140.
- [18] K. Lu, Gradient nanostructured materials, Acta Metall. Sin. 51 (2015) 1-10.
- [19] X.C. Liu, H.W. Zhang, K. Lu, Strain-induced ultrahard and ultrastable nanolaminated structure in nickel, Science 342 (2013) 337-340.
- [20] P.F. Wang, Z. Han, K. Lu, Enhanced tribological performance of a gradient nanostructured interstitial-free steel, Wear 402-403 (2018) 100-108.
- [21] X. Chen, Z. Han, X. Li, K. Lu, Friction and wear reduction in copper with a gradient nano-grained surface layer, ACS Appl. Mater. Interfaces 10 (2018) 13829-13838.
- [22] Y. Sun, Sliding wear behaviour of surface mechanical attrition treated AISI 304 stainless steel, Tribol. Int. 57 (2013) 67-75.
- [23] S.A. Kumar, S.G.S. Raman, T.S. Narayanan, R. Gnanamoorthy, Fretting wear behaviour of surface mechanical attrition treated alloy 718, Surf. Coat. Technol. 206 (2012) 4425-4432.
- [24] R.A. Bernal, R.W. Carpick, Visualization of nanoscale wear mechanisms in ultrananocrystalline diamond by in-situ TEM tribometry, Carbon 154 (2019) 132-139.
- [25] X. Hu, M.V.P. Altoe, A. Martini, Amorphization-assisted nanoscale wear during the running-in process, Wear 370-371 (2017) 46-50.
- [26] J.C. Walker, S.R. Saranu, A.H. Kean, R.J.K. Wood, Fe nano-particle coatings for

- high temperature wear resistance, Wear 271 (2011) 2067-2079.
- [27] G. Zhou, Y. Zhu, X. Wang, M. Xia, Y. Zhang, H. Ding, Sliding tribological properties of 0.45% carbon steel lubricated with Fe₃O₄ magnetic nano-particle additives in baseoil, Wear 301 (2013) 753-757.
- [28] H. Kato, K. Komai, Tribofilm formation and mild wear by tribo-sintering of nanometer-sized oxide particles on rubbing steel surfaces, Wear 262 (2007) 36-41.
- [29] K. Mondal, T. Ohkubo, T. Toyama, Y. Nagai, M. Hasegawa, K. Hono, The effect of nanocrystallization and free volume on the room temperature plasticity of Zr-based bulk metallic glasses, Acta Mater. 56 (2008) 5329-5339.
- [30] S. Pauly, S. Gorantla, G. Wang, U. Kühn, J. Eckert, Transformation-mediated ductility in CuZr-based bulk metallic glasses, Nat. Mater. 9 (2010) 473-477.
- [31] K. Wang, T. Fujita, Y.Q. Zeng, N. Nishiyam, A. Inoue, M.W. Chen, Micromechanisms of serrated flow in a Ni₅₀Pd₃₀P₂₀ bulk metallic glass with a large compression plasticity, Acta Mater. 56 (2008) 2834-2842.
- [32] B. Sarac, Y.P. Ivanov, A. Chuvilin, T. Schöberl, M. Stoica, Z. Zhang, J. Eckert, Origin of large plasticity and multiscale effects in iron-based metallic glasses, Nat. Commun. 9 (2018) 1333.
- [33] B.Q. Chen, Y. Li, R. Li, S.J. Pang, Y. Cai, H. Wang, T. Zhang, Influence of laser surface melting on glass formation and tribological behaviors of Zr₅₅Al₁₀Ni₅Cu₃₀ alloy, J. Mater. Res. 26 (2011) 2642-2652.
- [34] Z.L. Liao, N.B. Hua, W.Z. Chen, Y.T. Huang, T. Zhang, Correlations between the

- wear resistance and properties of bulk metallic glasses, Intermetallics 93 (2018) 290-298.
- [35]D. Maddala, R.J. Hebert, Effect of notch toughness and hardness on sliding wear of Cu₅₀Hf_{41.5}Al_{8.5} bulk metallic glass, Scripta Mater. 65 (7) (2011) 630-633.
- [36] S. Jahanmir, N.P. Suh, Mechanics of subsurface void nucleation in delamination wear, Wear 44 (1977) 17-38.
- [37] J.R. Fleming, N.P. Suh, Mechanics of crack propagation in delamination wear, Wear 44 (1977) 39-56.
- [38] E. Hornbogen, The role of fracture toughness in the wear of metals, Wear 33 (1975) 251-259.
- [39] M.N. Gardos, R.G. Hardisty, Fracture toughness- and hardness-dependent polishing wear of silicon nitride ceramics, Tribol. T. 36 (1993) 652-660.
- [40] N. Wanderka, E. Davidov, G. Miehel, V. Naundorf, M.P. Macht, J. Banhart, Crystallization of Pd₄₀Cu₃₀Ni₁₀P₂₀ bulk glass, J. Metast. Nanocryst. Mater. 20-21 (2004) 35-40.
- [41] K. Georgarakis, A.R. Yavari, D.V. Louzguine-Luzgin, G. Vaughan, Crystallization and vitrification of a PdCuNiP metallic glass upon thermal and mechanical processes detected by synchrotron light X-ray radiation, AIP Conf. Proc. 1518 (2013) 672-681.
- [42] A.R. Yavari, K. Georgarakis, J. Antonowicz, M. Stoica, N. Nishiyama, G. Vaughan, M.W. Chen, M. Pons, Crystallization during bending of a Pd-based metallic glass detected by X-ray microscopy, Phys. Rev. Lett. 109 (2012) 085501.

- [43] M.W. Chen, A. Inoue, W. Zhang, T. Sakurai, Extraordinary plasticity of ductile bulk metallic glasses, Phys. Rev. Lett. 96 (2006) 245505.
- [44] A. Inoue, W. Zhang, T. Tsurui, A.R. Yavari, A.L. Greer, Unusual room-temperature compressive plasticity in nanocrystal-toughened bulk copper-zirconium glass, Phil. Mag. Lett. 85 (2005) 221-237.
- [45] H. Chen, Y. He, G.J. Shiflet, S.J. Poon, Deformation-induced nanocrystal formation in shear bands of amorphous alloys, Nature 367 (1994) 541-543.
- [46] Z.J. Yan, K.K. Song, Y.Hu, F.P. Dai, Z.B. Chu, J. Eckert, Localized crystallization in shear bands of a metallic glass, Sci. Rep. 6 (2006) 19358.
- [47] B.Q. Chen, Y. Li, Y. Cai, R. Li, S.J. Pang, T. Zhang, Surface vitrification of alloys by laser surface treatment, J. Alloy. Compd. 511 (2012) 215-220.
- [48] R.F. Li, Z.G. Li, J. Huang, Y.Y. Zhu, Microstructure and wear properties of laser processed Ni based amorphous matrix coatings, Surf. Eng. 28 (2012) 513-516.
- [49] P.P. Zhang, Y.L. Lu, H. Yan, K. Ma, P.Q. Xu, Z.S. Yu, Y.Y. Chen, M. Ding, Effect of Nb addition on Fe-Ni-B-Si amorphous and crystalline composite coatings by laser processing, Surf. Coat. Tech. 236 (2013) 84-90.
- [50] Y. Guo, G.Y. Koga, A.M. Jorge Jr., S. Savoie, R. Schulz, C.S. Kiminami, C. Bolfarini, W.J. Bott, Microstructural investigation of Fe–Cr–Nb–B amorphous/nanocrystalline coating produced by HVOF, Mater. Design. 111 (2016) 608-615.
- [51] G.M. Hamilton, Explicit equations for the stresses beneath a sliding spherical contact, J. Mech. Eng. Sci. 197 (1983) 53-59.

- [52] Y.B. Zhang, G.C. Xiao, M.D. Yi, C.G. Xu, Effect of graphene orientation on microstructure and mechanical properties of silicon nitride ceramics, Process. Appl. Ceram. 12 (2018) 27-35.
- [53] J. Chen, S.J. Bull, On the relationship between plastic zone radius and maximum depth during nanoindentation, Surf. Coat. Tech. 201 (2006) 4289-4293.
- [54] K. Mishima, T. Otomo, K. Ikeda, H. Ohshita, Neutron scattering cross section of diamond nanoparticles, EPJ Web Conf. 219 (2019) 10005.
- [55] Y.X. Ye, C.Z. Liu, H. Wang, T.G. Nieh, Friction and wear behavior of a single-phase equiatomic TiZrHfNb high-entropy alloy studied using a nanoscratch technique, Acta Mater. 147 (2018) 78-89.
- [56]J.W. Kannel, S.A. Barber, Estimate of surface temperatures during rolling contact, Tribol. Trans. 32 (1989) 305-310.
- [57] U. Harms, T.D. Shen, R.B. Schwarz, Thermal conductivity of Pd₄₀Ni_{40-x}Cu_xP₂₀ metallic glasses, Scripta Mater. 47 (2002) 411-414.
- [58] N. Nishiyama, M. Horino, O. Haruyama, A. Inoue, Abrupt change in heat capacity of supercooled Pd-Cu-Ni-P melt during continuous cooling, Mater. Sci. Eng. A 304-306 (2001) 683-686.
- [59] H. Wu, I. Baker, Y. Liu, X. Wu, PR. Munroe, J. Zhang, Tribological studies of a Zr-based bulk metallic glass, Intermetallics 35 (2013) 25-32.
- [60] E.J. Pavlina, C.J. V. Tyne, Correlation of yield strength and tensile strength with hardness for steels, J. Mater. Eng. Perform. 17 (2008) 888-893.
- [61] Y.Y. Cheng, S.J. Pang, C. Chen, T. Zhang, Tailoring residual stress to achieve

large plasticity in $Zr_{55}Al_{10}Ni_5Cu_{30}$ bulk metallic glass, J. Alloys Compd. 690 (2017) 176-181.